ACS APPLIED MATERIALS & INTERFACES

Research Article

www.acsami.org

Poly(vinyl alcohol) Nanocomposites Filled with Poly(vinyl alcohol)-Grafted Graphene Oxide

Henry Kuo Feng Cheng,[†,‡] Nanda Gopal Sahoo,[†] Yan Pei Tan,[†] Yongzheng Pan,[†] Hongqian Bao,[†] Lin Li,*[,†] Siew Hwa Chan,[†] and Jianhong Zhao[‡]

[†]School of Mechanical and Aerospace Engineering, Nanyang Technological University, 50 Nanyang Avenue, Singapore 639798

[‡]Singapore Institute of Manufacturing Technology, 71 Nanyang Drive, Singapore 638075

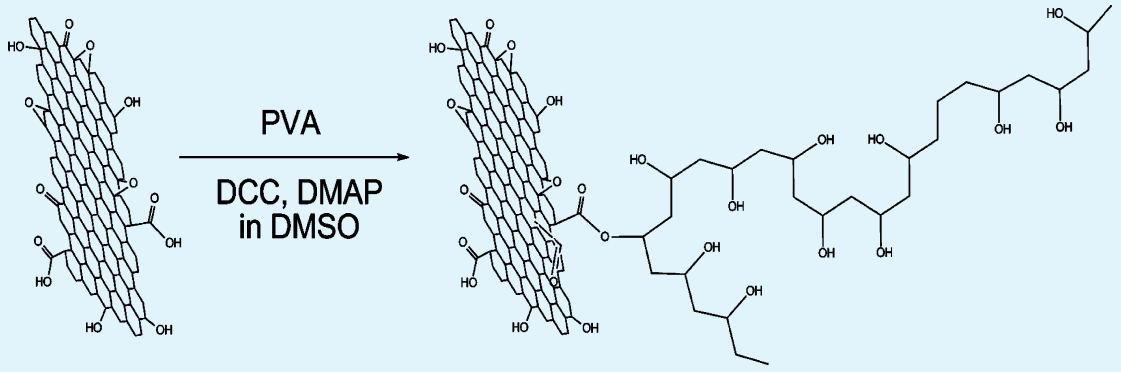

ABSTRACT: We present a novel approach to the fabrication of advanced polymeric nanocomposites from poly(vinyl alcohol) (PVA) by incorporation of PVA-grafted graphene oxide. In this work, we have synthesized PVA-grafted graphene oxide (PVA-g-GO) for the strong interfacial adhesion of graphene oxide (GO) to the PVA matrix. It was found that the mechanical properties of PVA were greatly improved by incorporating PVA-g-GO. For example, the tensile strength and Young's modulus of the PVA nanocomposite films containing 1 wt % net GO in the PVA-g-GO significantly increased by 88 and 150%, respectively, as compared to unfilled PVA. The elongation at break was also increased by 22%, whereas the GO/PVA nanocomposite containing 1 wt % pristine GO was decreased by 15%. Therefore, the presence of the PVA-g-GO in the PVA matrix could make the PVA not only stronger but also tougher. The strong interfacial adhesion between PVA-g-GO and the PVA matrix was attributed to the good compatibility between PVA-g-GO and the matrix PVA as well as the hydrogen-bonding between them.

KEYWORDS: *graphene oxide, functionalization, poly(vinyl alcohol), interfacial adhesion, nanocomposite*

1. INTRODUCTION

Recently, nanomaterials have been opening a wide window of applications due to their structural features and special properties on a nanometer scale.[1] To date, carbon-based nanofillers, such as carbon black (CB),[2−4] carbon nanotubes (CNTs),[5−9] graphene,[10−13] functionalized graphene,[14−16] and carbon nanofibers (CNF),[17−19] have been extensively used to prepare polymer nanocomposites. Among them, CNTs seem to be very effective fillers for reinforcement of polymers.[6,7] However, the major drawbacks of CNTs as nanofillers are the difficulty in dispersion in polymer matrices[6] and high production cost.[20] Recently, the development of graphene-based polymer nanocomposites has become a new direction of research in the area of polymer nanocomposites.[21] Graphene is an allotrope of carbon with a two-dimensional structure in which sp^2-bonded carbon atoms are densely packed in a honeycomb crystal lattice into a one-atom-thick planar sheet. Graphene possesses high thermal conductivity, superior mechanical strength, and excellent electronic conductivity.[22−25]

As compared with CNTs, graphene has become a relatively cheap nanomaterial because its synthesis procedure is much simpler than those methods used for synthesis of carbon nanotubes. It has been reported that the improvement in mechanical properties of polymers by adding graphene is much more efficient than that by nanoclay or other nanofillers.[21,26−28] Therefore, graphene is considered as a good choice of nanofillers for making advanced polymeric nanocomposites.[26−31]

The mechanical properties of a graphene-based polymeric nanocomposite greatly depend on the dispersion of graphene sheets in the polymeric matrix as well as interfacial bonding between graphene sheets and the polymeric matrix. However, because of the low compatibility of pristine graphene with most polymers as well as strong van der Waals interactions among graphene sheets, the dispersion of pristine graphene sheets in a polymer matrix is not individual and homogeneous. On the other hand, graphene oxide (GO) sheets, which are oxygenated graphene sheets, can have much lower van der Waals

Received: December 11, 2011
Accepted: April 10, 2012
Published: April 10, 2012

Scheme 1. Synthesis of PVA-g-GO Nanosheets

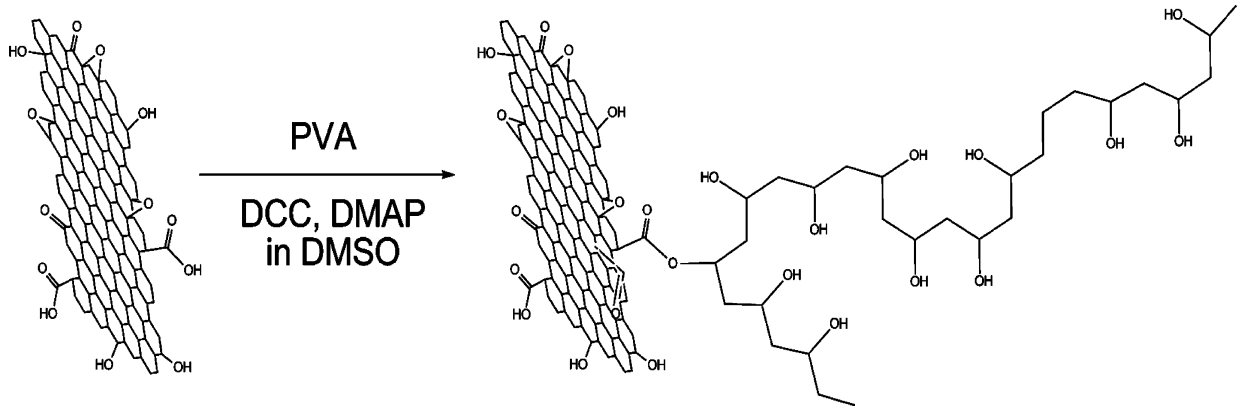

interactions among them than graphene sheets and be compatible with some polymers.[32−34] Moreover, due to the carbonyl and carboxyl groups located at their edges, GO sheets are hydrophilic, which allows them to be dispersed in water.[35,36]

Recently, Liang et al.[28] fabricated GO/PVA nanocomposites by using a solution method and reported that the load transfer between GO and PVA was efficient and the mechanical properties of GO/PVA composites were significantly improved because of the molecular-level dispersion of GO. A further better dispersion of GO in PVA would be expected if GO would contain the same type of groups on their surfaces as the polymer matrix.[6] However, the enhanced dispersion of GO in a PVA matrix by grafting GO with PVA chains, which is expected to significantly contribute to the improvement of mechanical properties of GO/PVA nanocomposites, has not been reported yet in the literature. The improved mechanical properties of such PVA-grafted GO/PVA nanocomposites will be achieved not only by the good dispersion of PVA-grafted GO in the PVA matrix but also by the strong interfacial adhesion between PVA-grafted GO and the matrix PVA.

Therefore, in this work, we have synthesized PVA-grafted GO (PVA-g-GO) and prepared PVA-g-GO/PVA nanocomposites using a solution method. The nanocomposites have been characterized in terms of their morphological, mechanical, and thermal properties in order to study the effects of the PVA modification of GO sheets on their dispersion in the PVA matrix and the interaction with the PVA. The properties of pristine-GO/PVA nanocomposite were also examined as a reference.

2. EXPERIMENTAL SECTION

2.1. Materials and Fabrication. The poly (vinyl alcohol) (PVA) with the trade name of Mowiol 10−98 was obtained from Sigma-Aldrich. It has an average molecular weight of 61 000 and is 98.0−98.8% hydrolyzed. The natural graphite powder with an average particle size of 100 μm was purchased from Fluka.

The GO nanosheets were synthesized from natural graphite powder using a modified Hummers method.[37] In this method, 3 g of natural graphite powder was added into a solution consisting of 12 mL of concentrated sulfuric acid (97%), 2.5 g of potassium persulfate, and 2.5 g of phosphorus pentoxide at 80 °C. The mixture was kept at 80 °C for 6 h. Then, the mixture was diluted with 0.5 L of deionized water and left to cool to room temperature (23 °C) overnight. The mixture was filtered with a 0.2 μm nylon filter and washed with deionized water to remove the residual acid. The product was dried at room temperature overnight. One g of the treated graphite and 0.5 g of sodium nitrate were put into a flask. Twenty-five ml of sulfuric acid (97%) was added with stirring into the flask kept in an ice−water bath and 3 g of potassium permanganate was slowly added for a course of 1 h. The mixture was then subjected to vigorous stirring at room temperature for 2 days. After then, 100 mL of 5 wt % aqueous sulfuric acid solution was added with stirring into the solution over a course of 1 h at 98 °C. The resultant mixture was further stirred at 98 °C for 2 h. Then, the temperature was reduced to 60 °C; 3 mL of 30 wt % aqueous hydrogen peroxide was added; and the mixture was stirred at room temperature for 2 h. The oxidation product was purified by rinsing with 10 wt % aqueous hydrochloric acid and large amount of deionized water while being filtered through a 0.2 μm Nylon filter.

Next, the GO nanosheets were functionalized with PVA by a carbodiimide-activated esterification reaction as shown in Scheme 1. The purified graphene oxide (GO, 50 mg) was dissolved and sonicated in dimethyl sulfoxide (DMSO, 15 mL) for 30 min to produce a homogeneous brown-colored solution. N,N′- dicyclohexylcarbodiimide (DCC, 2.3 g, 11 mmol) and 4-dimethylaminopyridine (DMAP, 0.17 g, 1.4 mmol) acted as catalysts in this reaction. They were stirred and added gradually for 10 min. A solution of PVA in DMSO (100 mg/mL, 5 mL) was then added and the resulting mixture was stirred at 50 °C for 3 days. Once this process was completed, the suspension was filtered through a 0.2 μm PTFE microporous membrane, and DMF and acetone were used to wash the residue thoroughly. To completely remove nonreacted PVA, the products were dissolved in hot water, and filtered with a 0.2 μm Nylon membrane. Finally, the filtrates were washed with hot water and the PVA-functionalized GO was dried in the vacuum oven at room temperature. In this study, the PVA-functionalized GO is named PVA-g-GO.

The preparation of PVA-g-GO/PVA composite samples followed the several steps. A solution of PVA-g-GO was first prepared by adding 50 mL of deionized water into 25 mg of PVA-g-GO, and the mixture was then sonicated in an ice-bath for 10 min at 30 W, 10 s interval. A PVA solution was prepared by adding 2 g of PVA into 20 mL of deionized water and then heating at 90 °C for 1 h in a flask. A certain volume ranging from 5 to 10 mL of PVA-g-GO solution, depending on the required weight percentage, was added dropwise into a respective volume of PVA solution. The solution was left on a stirrer for 15 min at room temperature. Finally, this homogeneous solution was poured onto a glass plate and was kept in a fume hood until dry at room temperature to form a 1 μm thick film of a PVA-g-GO/PVA composite. The similar procedure was also performed to fabricate the film of a GO/PVA nanocomposite. The fabricated films were cut into different shapes for the respective characterizations. The formulations and sample codes for the composites studied are tabulated in Table 1, where GO1/PVA is the composite consisting of 1 wt % pristine GO and 99 wt % PVA, whereas gGO1.4/PVA is the composite consisting of 1.4 wt % PVA-g-GO and 98.6 wt % PVA. As confirmed by thermogravimetry thermal analysis (TGA), the PVA-g-GO contains 30 wt % grafted PVA and 70 wt % GO. Therefore, the content of net GO in the gGO1.4/PVA is 1.0 wt %. The purpose of preparing the gGO1.4/PVA is to compare the effect of PVA-g-GO with pristine GO on the properties of PVA at the same loading (i.e., 1 wt %) of net GO.

Table 1. Sample Codes and Formulations

code	PVA (wt %)	PVA-g-GO[a] (wt %)	GO (wt %)
PVA	100		
GO1/PVA	99		1
gGO1.4/PVA	98.6	1.4	
gGO0.5/PVA	99.5	0.5	
gGO1/PVA	99.0	1.0	
gGO1.5/PVA	98.5	1.5	
gGO2/PVA	98.0	2.0	

[a]The PVA-g-GO contains 30 wt % grafted PVA and 70 wt % GO.

2.2. Characterization. Before being characterized, all the samples were dried at 60 °C for 12 h. According to the TGA analysis, the moisture content in all the samples was less than 2 wt % after drying. Fourier transform infrared (FTIR) spectrometry (Thermo Nicolet 6700 FTIR spectrometer) was used to characterize the PVA-g-GO at wavenumbers ranging from 600 to 4000 cm^{-1} and a resolution of 4 cm^{-1} and 16 scans. An atomic force microscope (Digital Instruments Dimension 3100 AFM) was used to obtain the images of GO sheets and PVA-g-GO sheets. The surface morphology of the tensile fractured samples was observed by field emission scanning electron microscopy (FESEM, JEOL JSM-5800), after gold coating. Tensile tests were carried out for the composite film samples on an Instron machine (Instron 5569) at room temperature with an extension speed of 5 mm/min and an initial gauge length of 35 mm. For each composite sample, five measurements were repeated and the average value was calculated. Thermal stability of the nanocomposites was examined up to 600 °C under dry nitrogen using thermogravimetry thermal analysis (TGA 2950 with a TA 500 controller from TA Instruments) at a temperature scan rate of 10 °C/min. Differential scanning calorimetric (DSC) measurements were carried out under dry nitrogen using a DSC analyzer (DSC-Q200, TA Instruments) from 40 to 250 °C at 10 °C/min.

3. RESULTS AND DISCUSSION

3.1. Functionalization of GO with PVA. The functionalization of GO nanosheets with PVA was confirmed by FTIR spectroscopy as shown in Figure 1. After GO was grafted with

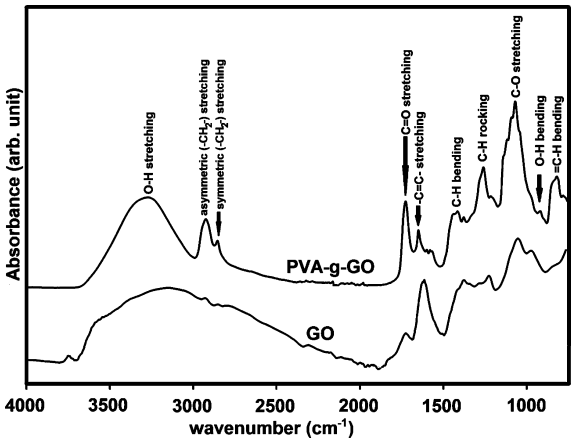

Figure 1. Fourier transform infrared (FTIR) spectra for GO and PVA-g-GO sheets.

PVA, an IR peak at 1750 cm^{-1} for the C═O stretching vibration of carboxylic acid groups appeared. The peaks of PVA-g-GO emerged at a considerably higher intensity as compared to GO. This can be seen from the peaks of C═O and C−O stretches at wavenumbers of 1750 and 1140 cm^{-1}, respectively. Beside the increased intensity of these peaks, the new ones were also observed. The wide-ranging peak between 3000 and 3600 cm^{-1} is attributed to O−H stretching, while those at 2940 and 2845 cm^{-1} represent ($-CH_2-$) asymmetric and symmetric stretching, respectively. The increased peak intensity and the formation of new peaks indicated that GO has been functionalized by PVA.

After PVA was grafted onto GO nanosheets, TGA was used to measure the content of grafted PVA on GO. From the thermograph in Figure 2, the percentage weight loss for pristine

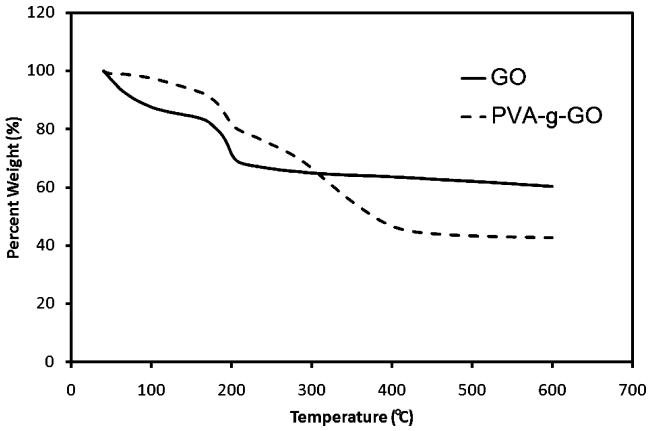

Figure 2. TGA curves of the pristine GO (solid line) and the PVA-g-GO (dotted line) at a heating rate of 10 °C/min.

GO at 600 °C was about 42%, whereas for the PVA-g-GO, it was about 60%. On the basis of this result, there was about 30 wt % PVA and 70 wt % GO in the PVA-g-GO. Therefore, it was confirmed that 30 wt % PVA had been grafted on the surfaces of GO.

The images of GO sheets and PVA-g-GO sheets obtained by the atomic force microscopic (AFM) measurements are shown in Figure 3. As observed in Figure 3, the GO exists as micrometer-sized platelets, whereas the PVA-g-GO sheets are of 0.5−1.5 μm in size because of the size reduction by the repeated sonication during the synthesis. The GO sheets had a thickness of about 1.5−2.0 nm with very sharp edges and flat surface. Therefore, we can conclude that our GO sheets were exfoliated into 2 to 3 layers . In contrast, the thickness of PVA-g-GO was increased to about 3.0−5.0 nm and the edges of PVA-g-GO appeared to be relatively rough and some protuberances were present on the surfaces, which were formed by wrapping and folding of PVA chains on the GO surface.

3.2. Dispersion of GO in PVA and Molecular Interactions at Interface. Figure 4 shows the FESEM micrographs for the cross-sectional fracture surfaces of the GO1/PVA and gGO1.4/PVA nanocomposites both containing 1.0 wt % of net GO. The images exhibit that the majority of the GO and PVA-g-GO nanosheets were well dispersed in the PVA matrix. The dispersion of these nanosheets looked random and not aligned parallel to the surfaces of the sample films. Although the dispersion of PVA-g-GO sheets was expected to be better than GO sheets, it is impossible to distinguish the difference in dispersion between GO and PVA-g-GO sheets in the PVA matrix from the FESEM images shown in Figure 4. From, the FESEM images of PVA-g-GO at lower (Figure 4c) and the higher (Figure 4d) magnifications, it is also clearly seen that the PVA-g-GO nanosheets were well dispersed in the PVA matrix. Besides, from Figure 4 (d), the thickness of PVA-g-GO

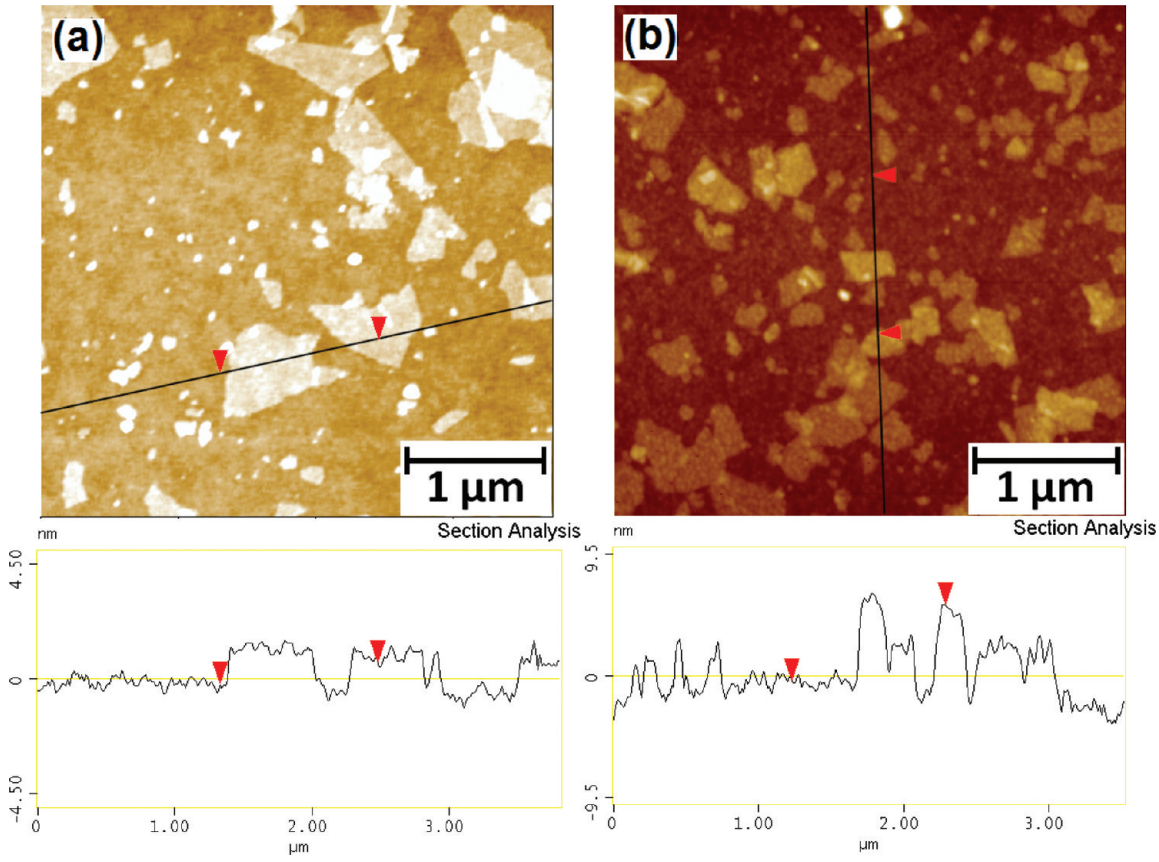

Figure 3. AFM images of (a) GO sheets and (b) PVA-g-GO sheets.

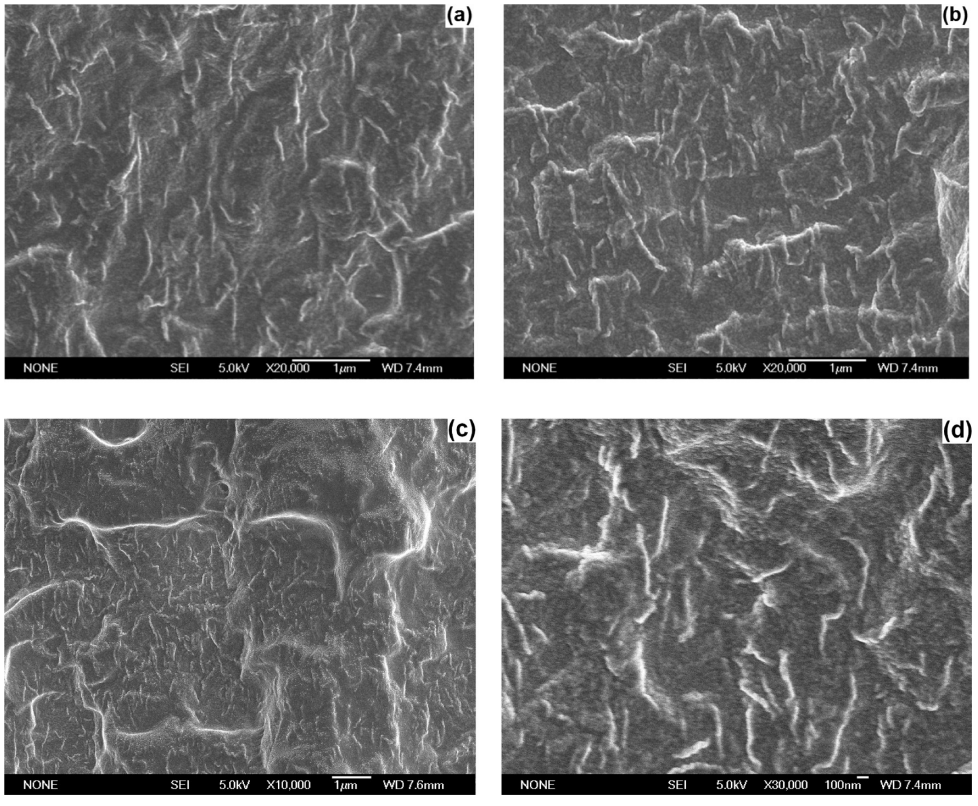

Figure 4. FESEM micrographs of the cross-section of (a) GO1/PVA and (b) gGO1.4/PVA composites at 20K magnifications and (c) gGO1.4/PVA composites at lower (10K) and (d) at higher (30K) magnifications.

sheets seems to be thicker than that observed from AFM. This is because the better compatibility of PVA-g-GO sheets with the PVA matrix makes them fully wetted with the matrix molecules after the solution-mixing with PVA.

The nature of molecular interaction between chemical groups on GO surfaces and the matrix PVA can be investigated by measuring the extent of shift in FTIR spectrum for the key groups on the GO and the matrix polymer after mixing. Figure 5 shows the FTIR spectra of PVA, GO1/PVA, and gGO1.4/

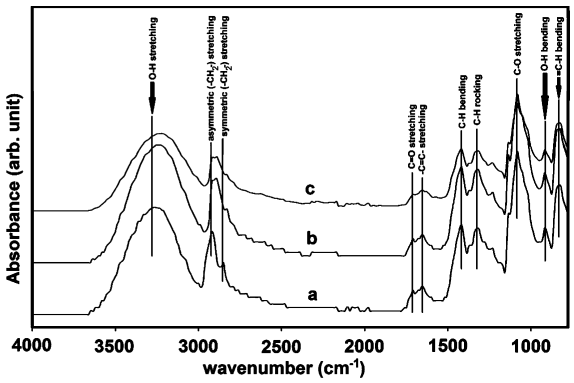

Figure 5. FTIR spectra of (a) PVA, (b) GO1/PVA, and (c) gGO1.4/PVA nanocomposites.

PVA nanocomposites. The FTIR spectra of PVA we obtained are in good agreement with the literature.[38] The wide and intense band peaked at 3260 cm^{-1} is attributed to the presence of hydroxyl group (−OH).[39] The bands corresponding to the asymmetric and symmetric stretching of $-CH_2-$ groups are located at 2950 and 2854 cm^{-1}, respectively. The peaks at 1455 and 1365 cm^{-1} can be attributed to C−H bending and rocking, respectively. The peak at 1140 cm^{-1} results from the stretching of C−O groups. From Figure 5, it can be clearly seen that the peak for −OH stretching shifted from 3260 cm^{-1} in the pure PVA to the lower wavenumbers of 3247 and 3245 cm^{-1} in the GO1/PVA and gGO1.4/PVA nanocomposites, respectively. Besides, the peaks for asymmetric and symmetric stretching of the $(-CH_2-)$ groups also shifted to the lower wavenumbers in both GO1/PVA and gGO1.4/PVA nanocomposites as compared to those of pure PVA. The results indicate that there are strong molecular interactions between the PVA and the GO (or PVA-g-GO). The strong molecular interactions at the filler−matrix interface are mainly attributed to the hydrogen bonding between the oxygen containing groups (e.g., hydroxyl, carboxyls, and epoxides) on the GO (or PVA-g-GO) and the −OH groups of PVA chains.

3.3. Thermal Properties of GO/PVA and GO-PVA/PVA Nanocomposites. To understand how the PVA-g-GO could affect on the glass transition behavior of the matrix polymer in the nanocomposites, differential scanning calorimetry (DSC) analysis was performed. Table 2 lists the glass transition, melting and crystallization temperatures of PVA in the nanocomposites. It can be found that both melting temperature (T_m) and crystallization temperature (T_c) of PVA in the nanocomposites increase with increasing PVA-g-GO content.

Figure 6 shows the glass transition behaviors of PVA alone and in the nanocomposites. The unfilled PVA shows a glass transition temperature (T_g) of 72.2 °C. At a fixed loading of 1 wt % net GO, T_g of PVA increases from 72.2 to 75.9 °C for the GO1/PVA composite containing the pristine GO and to 79.5

Table 2. Thermal Properties of Pure PVA, GO1/PVA, and gGO/PVA Composites

sample name	T_g (°C)	T_m (°C)	T_c (°C)
PVA	72.2	211.8	196.0
GO1/PVA	75.9	212.0	200.4
gGO1.4/PVA	79.5	222.7	202.8
gGO0.5/PVA	74.5	220.4	198.4
gGO1/PVA	75.9	221.6	201.5
gGO1.5/PVA	80.3	222.8	203.2
gGO2/PVA	78.5	223.0	203.5

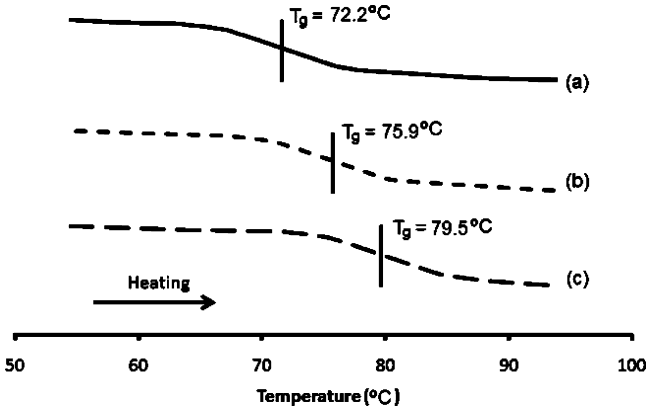

Figure 6. Glass transition temperature (T_g) at a heating rate of 10 °C/min for (a) PVA, (b) GO1/PVA, and (c) gGO1.4/PVA nanocomposites.

°C for the gGO1.4/PVA composite containing the PVA-g-GO. The reason for the increase in glass transition temperature for the GO1/PVA composite is because of the reduced mobility of polymer chains[40] by solid nanofiller sheets and H-bonding between oxygen-containing groups on the GO sheets and the hydroxyl groups of PVA chains.[27] These factors are also valid in the gGO1.4/PVA composite. The additional factor for the increase in glass transition temperature for the gGO1.4/PVA composite over the GO1/PVA composite is considered to be the miscibility between the PVA-grafted GO and the matrix PVA. The good miscibility between the PVA-grafted GO and the matrix PVA allows the GO sheets to be dispersed individually and homogeneously, which could maximize the fillers' effect on reducing mobility of polymer chains. At the same time, the strong interfacial adhesion between the PVA-grafted GO and the matrix PVA due to the good miscibility ensures an efficient load transfer at the interface. As a result, T_g is further increased. The similar results could be found in the literature. For example, Viswanathan et al. reported that the addition of only 0.05 wt % polystyrene-grafted single-walled carbon nanotubes into the polystyrene matrix increased the glass transition temperature by 15 °C.[41]

A number of publications[2,6,7] also reported that both glass transition temperature (T_g) and the melting temperature (T_m) of a polymer are enhanced in the presence of rigid nanofillers due to their restriction on the mobility of the matrix polymer molecules.

Figure 7 shows the comparison of thermal stability among pure PVA, GO1/PVA, and gGO1.4/PVA composites. It is seen from Figure 7 that, the addition of PVA-g-GO into PVA made PVA more thermally stable than that of pristine GO into PVA at the same loading of 1 wt % net GO. The main reason why the gGO/PVA composites exhibited the better thermal

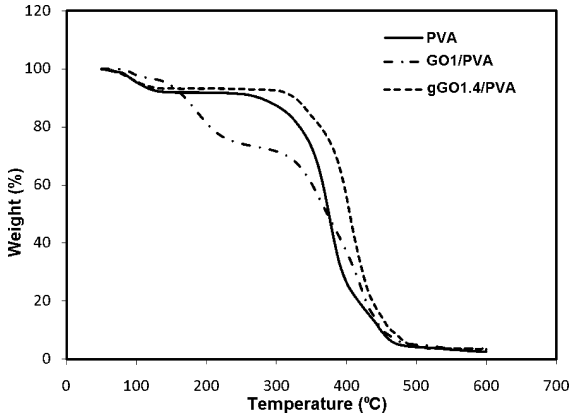

Figure 7. TGA curves for PVA, GO1/PVA, and gGO1.4/PVA at a heating rate of 10 °C/min.

stabilities than the pure PVA is the interfacial interactions between the components in the composites. Because of the H-bonding between the PVA-g-GO and the PVA chains as well as the miscibility between the PVA-g-GO and the matrix PVA, the interfacial adhesion between PVA-g-GO and PVA are stronger than those between GO and PVA. Thus, the gGO/PVA composites show the higher thermal stability than the GO/PVA composites.

3.4. Mechanical Properties of GO/PVA and GO-PVA/PVA Nanocomposites. The general purpose of incorporating a small amount of GO sheets into a polymer matrix is to improve its mechanical properties. At the same loading of net GO, the PVA-g-GO is expected to contribute more efficiently to the improvement in mechanical properties of PVA than pristine GO does. This is because of the stronger interfacial adhesion between PVA-g-GO and the matrix PVA, which is obtained from both the hydrogen-bonding between the PVA-g-GO and the matrix PVA as well as the better miscibility between them, as compared to pristine GO. To verify this hypothesis, we obtained the typical stress−strain curves for the films of PVA, GO1/PVA nanocomposite and gGO1.4/PVA nanocomposite and presented in Figure 8 and Table 3. From Figure 8 and Table 3, we know that the tensile strength and Young's modulus of GO1/PVA nanocomposite significantly increased by 30% and 80%, respectively, as compared to pure

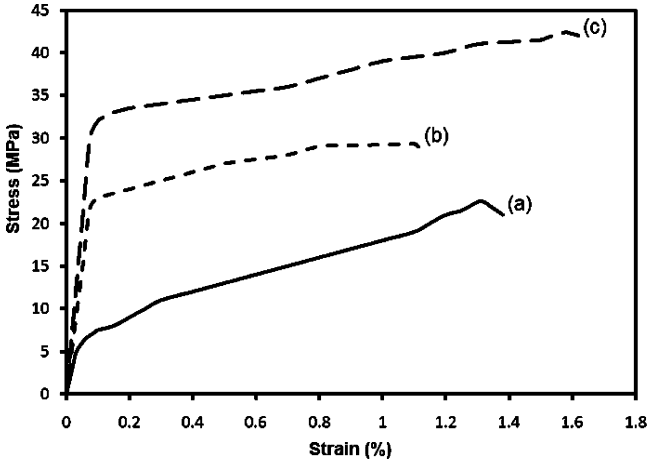

Figure 8. Stress−strain curves of (a) PVA, (b) GO1/PVA nanocomposite, and (c) gGO1.4/PVA nanocomposite.

Table 3. Mechanical Properties of Pure PVA, GO1/PVA, and gGO/PVA Composites

sample code	vol % GO in PVA-g-GO	tensile strength (MPa)	Young's modulus (GPa)	strain at break (%)
PVA		22.5 ± 0.83	0.16 ± 0.025	130 ± 4.95
GO1/PVA	0.6	29.3 ± 1.5	0.29 ± 0.042	110 ± 5.40
gGO1.4/PVA	0.6	42.4 ± 1.6	0.40 ± 0.021	158 ± 4.48
gGO0.5/PVA	0.21	32.1 ± 0.93	0.25 ± 0.01	167 ± 5.53
gGO1/PVA	0.42	38.4 ± 1.4	0.32 ± 0.015	162 ± 4.81
gGO1.5/PVA	0.63	43.8 ± 1.6	0.43 ± 0.026	155 ± 5.46
gGO2/PVA	0.84	45.7 ± 1.8	0.53 ± 0.041	147 ± 4.91

PVA, but the elongation at break slightly decreased by 15%. On the other hand, for the gGO1.4/PVA nanocomposite, the tensile strength and elastic modulus increased by 88% and 150%, respectively from pure PVA, and the elongation at break also increased by 22%. Therefore, the incorporation of the PVA-g-GO in the PVA matrix resulted in not only stronger but also tougher PVA composites than PVA and GO/PVA composites.

Further, let us study the effect of PVA-g-GO content on mechanical properties of PVA. The mechanical properties of all gGO/PVA composites are listed in Table 3. Here the volume fractions of net GO in the composites were calculated using the densities of PVA and graphene oxide nanosheets, which were taken as 1.3 and 2.2 g/cm^3, respectively.[42,43] Figure 9 represents

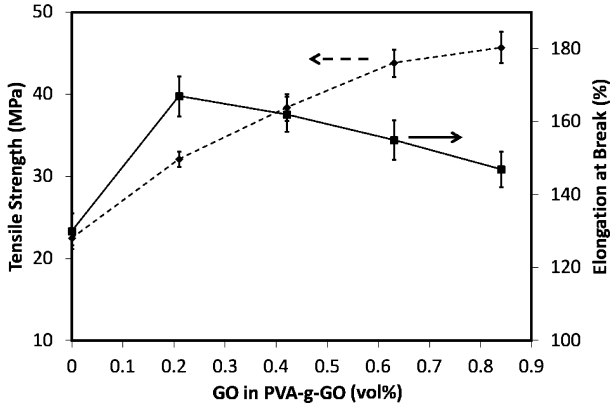

Figure 9. Mechanical properties of gGO/PVA nanocomposites: tensile strength (dotted line, left axis) and elongation at break (solid line, right axis) versus GO loadings in the PVA-g-GO.

the relationship between PVA-g-GO loading and the tensile properties of the gGO/PVA nanocomposites. It is observed in Figure 9 that the tensile strength of the gGO/PVA nanocomposites increases monotonously with increasing content of PVA-g-GO. For example, the addition of 0.5 wt % (0.21 vol % net GO) PVA-g-GO into the matrix resulted in the increases in tensile strength by 43% and elongation at break by 40% from pure PVA. At the highest loading (2 wt % PVA-g-GO or 0.84 vol % net GO) of PVA-g-GO used in this study, the tensile strength reached to 45.7 MPa, which is two times that (22.5 MPa) of the pure PVA. The elongation at break reached the maximum at 0.21 vol % of net GO, and then decreased linearly with increasing GO content, indicating a well-known negative

effect of solid fillers on ductility of filler/polymer composites. However, it is interesting to note that although the elongation at break decreased from the maximum (167%) at 0.21 vol % net GO to 147% at 0.84 vol % net GO, all the values of elongation at break are still higher than that (130%) of pure PVA, which is not generally observed from other filler-reinforced polymer composites, including the GO/PVA composite (i.e., GO1/PVA) shown in Table 3 and Figure 8. The enhanced ductility of PVA by adding the PVA-g-GO is considered to be due to the strong interfacial adhesion between the PVA-g-GO and the PVA matrix. The results of elongation at break are a strong evidence that the interfacial adhesion between pristine GO and the PVA matrix is not as strong as that between the PVA-g-GO and the same matrix.

To predict the Young's modulus of unidirectional or randomly distributed filler-reinforced nanocomposites, the Halpin–Tsai model[44−47] is widely used in the literature. We also use this model to predict the Young's modulus for the gGO/PVA nanocomposites. For the moduli of randomly oriented or unidirectional GO in the polymer matrix, the Halpin–Tsai model gives E_{random} and $E_{parallel}$, as described in the following set of equations.

$$E_{random} = E_{PVA}\left[\frac{3}{8}\frac{1 + (2L_{GO}/3T_{GO})(\eta_L V_{GO})}{1 - (\eta_L V_{GO})} + \frac{5}{8}\frac{1 + (2\eta_T V_{GO})}{1 - (\eta_T V_{GO})}\right] \quad (1)$$

$$E_{parallel} = E_{PVA}\left[\frac{1 + (2L_{GO}/3T_{GO})(\eta_L V_{GO})}{1 - (\eta_L V_{GO})}\right] \quad (2)$$

$$\eta_L = \frac{(E_{GO}/E_{PVA}) - 1}{(E_{GO}/E_{PVA}) + (2L_{GO}/3T_{GO})} \quad (3)$$

$$\eta_T = \frac{(E_{GO}/E_{PVA}) - 1}{(E_{GO}/E_{PVA}) + 2} \quad (4)$$

where E_{random} and $E_{parallel}$ represent the Young's modului of a GO/PVA nanocomposite with randomly distributed GO and aligned GO parallel to the sample surface, respectively. E_{GO} and E_{PVA} are the Young's moduli of the GO and the PVA matrix, respectively. L_{GO} and T_{GO} refer to the length and thickness of GO, and V_{GO} is the volume fraction of GO in the nanocomposites. The Young's modulus of the chemically reduced monolayer graphene oxide was previously reported as around 0.25 TPa,[48] which may be approximately similar to that of the GO sheets in the PVA-g-GO used in this study. The Young's modulus of pure PVA is 0.16 GPa from the experimental data. The statistical average values of L_{GO} and T_{GO} were about 1.0 μm and 4.0 nm, respectively, as determined by AFM analysis. Substituting these parameters into eqs 2–5, the Young's modulus of the nanocomposite was calculated under two assumptions: (i) GO sheets were aligned parallel to the sample surface and (ii) GO sheets were randomly dispersed throughout the sample.

As shown in Figure 10, a good agreement was found between the experimental data obtained for the gGO/PVA nanocomposites and the theoretical predictions under the hypothesis that GO sheets were randomly dispersed throughout the sample. However, the deviation of the experimental curve from the theoretical prediction with randomly oriented

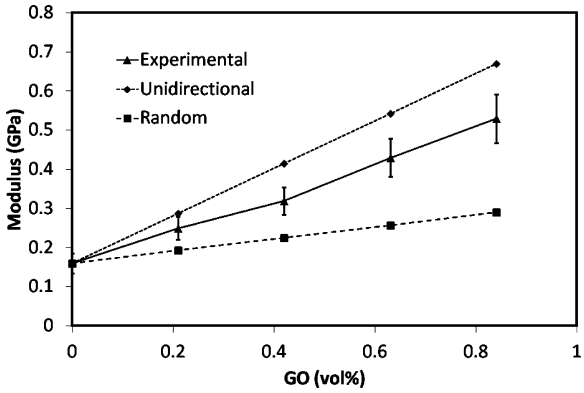

Figure 10. Experimental Young's moduli of the PVA-g-GO/PVA composites and those calculated using Halpin–Tsai models with two extreme cases: the random orientation and unidirectional dispersion of PVA-g-GO sheets in the PVA matrix.

PVA-g-GO sheets toward the theoretical one with unidirectionally oriented PVA-g-GO sheets may indicate that not all of the PVA-g-GO sheets in the samples were fully randomly oriented. In other words, some of PVA-g-GO sheets might be oriented parallel to the sample surface. The reinforcing mechanism of the gGO/PVA composites could be due to the effective load transfer between the PVA matrix and PVA-g-GO via strong interfacial adhesion.

4. CONCLUSIONS

The GO sheets were chemically grafted with PVA before being incorporated into a PVA matrix. Then, the pristine GO sheets and the PVA-grafted GO sheets were separately mixed with PVA in an aqueous solution to fabricate GO/PVA nanocomposites. The FESEM micrographs confirmed the homogeneous dispersion of PVA-g-GO sheets in the PVA-g-GO/PVA nanocomposites. The PVA-g-GO/PVA nanocomposites were found to be much stronger and also tougher than PVA. Moreover, a good agreement was obtained between the experimental and the theoretical prediction by the Halpin–Tsai hypothesis: the majority of PVA-grafted GO sheets were randomly dispersed throughout the composite films. The reinforcing mechanism of the PVA-g-GO/PVA composites is considered to be due to the effective load transfer between the PVA matrix and PVA-g-GO sheets via the strong interfacial adhesion between them.

AUTHOR INFORMATION

Corresponding Author

*Corresponding author. Tel: +65-6790 6285, Fax: +65-6791 1859, Email: mlli@ntu.edu.sg.

Notes

The authors declare no competing financial interest.

REFERENCES

(1) Okada, A.; Kawasumi, M.; Usuki, A.; Kojima, Y.; Kurauchi, T.; Kamigaito, O. In: *Polymer Based Molecular Composites*, Schaefer, D. W., Mark, J. E., Eds.; MRS Symposium Proceedings; Materials Research Society: Warrendale, PA, 1990; Vol. *171*, p 45.

(2) Cheng, H. K. F.; Sahoo, N. G.; Pan, Y.; Li, L.; Chan, S. H.; Zhao, J.; Chen, G. *J Polym Sci Part B* **2010**, *48*, 1203–1212.

(3) Jeevananda, T.; Jang, Y. K.; Lee, J. H.; Siddaramaiah, M. V.; Ranganathaiah, C. *Polym. Int.* **2009**, *58*, 755–780.

(4) Li, Q.; Siddaramaiah; Kim, N. H.; Yoo, G. H.; Lee, J. H. *Compos., Part B* **2009**, *40*, 218–224.

(5) Li, H.; Cheng, F.; Duft, A. M.; Adronov, A. *J. Am. Chem. Soc.* **2005**, *127*, 14518−14524.
(6) Sahoo, N. G.; Cheng, H. K. F.; Li, L.; Chan, S. H.; Judeh, Z.; Zhao, J. *Adv. Funct. Mater.* **2009**, *19*, 3962−3971.
(7) Sahoo, N. G.; Cheng, H. K. F.; Cai, J.; Li, L.; Chan, S. H.; Zhao, J.; Yu, S. *Mater. Chem. Phys.* **2009**, *117*, 313−320.
(8) Gao, J.; Itkis, M. E.; Yu, A.; Bekyarova, E.; Zhao, B.; Haddon, R. C. *J. Am. Chem. Soc.* **2005**, *127*, 3847−3854.
(9) Campidelli, S.; Sooambar, C.; Diz, E. L.; Ehli, C.; Guldi, D. M.; Prato, M. *J. Am. Chem. Soc.* **2006**, *128*, 12544−12552.
(10) Wang, H.; Zhang, H.; Zhao, W.; Zhang, W.; Chen, G. *Compos. Sci. Technol.* **2008**, *68*, 238−243.
(11) Yu, A.; Ramesh, P.; Itkis, M. E.; Elena, B.; Haddon, R. C. *J. Phys. Chem. C* **2007**, *111*, 7565−7569.
(12) Debelak, B.; Lafdi, K. *Carbon* **2007**, *45*, 1727−1734.
(13) Chen, X.; Zheng, Y. P.; Kang, F.; Shen, W. C. *J. Phys. Chem. Solids* **2006**, *67*, 1141−1144.
(14) Ansari, S.; Giannelis, E. P. *J. Polym. Sci., Part B* **2009**, *47*, 888−897.
(15) Ramanathan, T.; Abdala, A. A.; Stankovich, S.; Dikin, D. A.; Herrera-Alonso, M.; Piner, R. D.; Adamson, D. H.; Schniepp, H. C.; Chen, X.; Ruoff, R. S.; Nguyen, S. T.; Aksay, I. A.; Prud'Homme, R. K.; Brinson, L. C. *Nat. Nanotechnol.* **2008**, *3*, 327−331.
(16) Lee, Y. R.; Raghu, A. V.; Jeong, H. M.; Kim, B. K. *Macromol. Chem. Phys.* **2009**, *210*, 1247−54.
(17) Khanna, V.; Bakshi, B. R. *Environ. Sci. Technol.* **2009**, *43*, 2078−2084.
(18) Tibbetts, G. G.; Lake, M. L.; Strong, K. L.; Rice, B. P. *Compos. Sci. Technol.* **2007**, *67*, 1709−1718.
(19) Chipara, M.; Lozano, K.; Hernandez, A.; Chipara, M. *Polym. Degrad. Stab.* **2008**, *93*, 871−876.
(20) Liu, N.; Luo, F.; Wu, H.; Liu, Y.; Zhang, C.; Chen, J. *Adv. Funct. Mater.* **2008**, *18*, 1518−1525.
(21) Stankovich, S.; Dikin, D. A.; Dommett, G. H. B.; Kohlhaas, K. M.; Zimney, E. J.; Stach, E. A.; Stach, E. A.; Piner, R. D.; Nguyen, S. T.; Ruoff, R. S. *Nature* **2006**, *442*, 282−286.
(22) Dreyer, R. D.; Park, S.; Bielawski, C. W.; Ruoff, R. S. *Chem. Soc. Rev.* **2010**, *39*, 228−240.
(23) Wang, G.; Shen, X.; Wang, B.; Yao, J.; Park, J. *Carbon* **2009**, *47*, 1359−1364.
(24) Li, X.; Wang, X.; Zhang, L.; Lee, S.; Dai, H. *Science* **2008**, *319*, 1229−1232.
(25) Blake, P.; Brimicombe, P. D.; Nair, R. R.; Booth, T. J.; Jiang, D.; Schedin, F.; Ponomarenko, L. A.; Morozov, S. V.; Gleeson, H. F.; Hill, E. W.; Geim, A. K.; Novoselov, K. S. *Nano Lett* **2008**, *8*, 1704−1708.
(26) Putz, K. W.; Compton, O. C.; Palmeri, M. J.; Nguyen, S. T.; Brinson, L. C. *Adv. Funct. Mater.* **2010**, *20*, 3322−3329.
(27) Kim, H.; Macosko, C. W. *Polymer* **2009**, *50*, 3797−3809.
(28) Liang, J.; Huang, Y.; Zhang, L.; Wang, Y.; Ma, Y.; Guo, T.; Chen, Y. *Adv. Funct. Mater.* **2009**, *19*, 2297−2302.
(29) Mahmoud, W. E. *Eur. Polym. J.* **2011**, *47*, 1534−1540.
(30) Kuilla, T.; Bhadra, S.; Yao, D.; Kim, N. H.; Bose, S.; Lee, J. H. *Prog. Polym. Sci.* **2010**, *35*, 1350−1375.
(31) Sengupta, R.; Bhattacharya, M.; Bandyopadhyay, S.; Bhowmick, A. K. *Prog. Polym. Sci.* **2011**, *36*, 638−670.
(32) Becerril, H. A.; Mao, J.; Liu, Z.; Stoltenberg, R. M.; Bao, Z.; Chen, Y. *ACS Nano* **2008**, *2*, 463−70.
(33) Dikin, D. A.; Stankovich, S.; Zimney, E. J.; Piner, R. D.; Dommett, G. H. B.; Evmenenko, G.; Nguyen, S. T.; Ruoff, R. S. *Nature* **2007**, *448*, 457−460.
(34) Vickery, L.; Patil, A. J.; Mann, S. *Adv. Mater.* **2009**, *21*, 2180−2184.
(35) Nethravathi, C.; Rajamathi, J. T.; Ravishankar, N.; Shivakumara, C.; Rajamathi, M. *Langmuir* **2008**, *24*, 8240−8244.
(36) Szabo, T.; Szeri, A.; Dekany, I. *Carbon* **2005**, *43*, 87−94.
(37) Kovtyukhova, N. I.; Ollivier, P. J.; Martin, B. J.; Mallouk, T. E.; Chizhik, S. A.; Buzaneva, E. V.; Gorchinskiy, A. D. *Chem. Mater.* **1999**, *11*, 771−778.
(38) Wang, T.; Turhan, M.; Gunasekaran, S. *Polym. Int.* **2004**, *53*, 911−918.
(39) Yang, X.; Li, L.; Shang, S.; Tao, X. *Polymer* **2010**, *51*, 3431−3435.
(40) Mbhele, Z. H.; Salemane, M. G.; Sittert, C.; Nedeljkovic, J. M.; Djokovic, V.; Luyt, A. S. *Chem. Mater.* **2003**, *15*, 5019−5024.
(41) Viswanathan, G.; Chakrapani, N.; Yang, H.; Wei, B.; Chung, H.; Cho, K.; Ryu, C. Y.; Ajayan, P. M. *J. Am. Chem. Soc.* **2003**, *125*, 9258−9259.
(42) Stankovich, S.; Dinkin, D. A.; Dommett, G. H. B.; Kohlhaas, K. M.; Zimney, E. J.; Stach, E. A.; Pinner, R. D.; Nguyen, S. T.; Ruoff, R. S. *Nature* **2006**, *442*, 282−286.
(43) Zhao, X.; Zhang, Q.; Chen, D.; Lu, P. *Macromolecules* **2010**, *43*, 2357−2363.
(44) Tiwari, R. R.; Khilar, K. C.; Natarajan, U. *J. Appl. Polym. Sci.* **2008**, *108*, 1818−1828.
(45) Kalaitzidou, K.; Fukushima, H.; Miyagawa, H.; Drzal, L. T. *Polym. Eng. Sci.* **2007**, *47*, 1796−1803.
(46) Schaefer, D. W.; Justice, R. S. *Macromolecules* **2007**, *40*, 8501−8517.
(47) Halpin, J. C.; Kardos, J. L. *Polym. Eng. Sci.* **1976**, *16*, 344−352.
(48) Gomez-Navarro, C.; Burghard, M.; Kern, K. *Nano Lett.* **2008**, *8*, 2045−2049.